https://doi.org/10.48048/tis.2024.7142

The Implementation of Response Surface Methodology in the Optimization of Lipid Nanoparticle Preparation for Vaccine Development

Muhamad Abidin[1,2], Muhammad Yusuf[1,2,3], Wahyu Widayat[1,4], Toto Subroto[1,2,3], Neni Nurainy[5] and Ari Hardianto[2,3,*]

[1]Departement of Biotehnology, School of Postgraduate, Universitas Padjadjaran, West Java 40132, Indonesia
[2]Research Centre for Molecular Biotechnology and Bioinformatics, Universitas Padjadjaran, Jawa Barat 40132, Indonesia
[3]Departement of Chemistry, Universitas Padjadjaran, West Java 45363, Indonesia
[4]Facutly of Pharmacy, Universitas Mulawarman, Kalimantan Timur 75119, Indonesia
[5]PT Bio Farma, West Java 40161, Indonesia

([*]Corresponding author's email: a.hardianto@unpad.ac.id)

Received: 29 May 2023, Revised: 28 June 2023, Accepted: 29 June 2023, Published: 1 November 2023

Abstract

Lipid nanoparticles (LNPs) are the delivery system behind the success story of mRNA vaccines and the development of DNA and peptide vaccines. LNPs should have particle sizes ranging from 60 to 150 nm for such applications. Achieving such particle size criteria can be challenging in the LNP preparation using a micromixer system with different parameters: i.e., the N/P ratio, aqueous flow rate (AFR) and total flow rate (TFR). Such an issue can be addressed by applying response surface methodology (RSM). Therefore, in this study, we implemented RSM to optimize LNP preparation parameters, including the N/P ratio and AFR. TFR remained constant at 1 mL.min^{-1} since, from a previous study, it is not a critical parameter for achieving the desired LNP size. Here, we used the pDNA of ACE-2 as a dummy nucleotide. Particle sizes of the resulting LNPs were determined using a dynamic light scattering (DLS) method. Our results indicate that AFR is a significant factor in determining LNP size, whereas the N/P ratio does not have a significant impact on LNP size. We achieved an LNP size of 104.00 nm by applying the N/P ratio of 32.0000 and AFR of 0.9621 mL.min^{-1}. Our results showed that RSM could ease the optimization process in the preparation of LNP, which may support the acceleration of vaccine development.

Keywords: Aqueous flow rate, Lipid nanoparticles, Particle size, Response surface methodology, N/P ratio

Introduction

LNPs have many applications, such as in drug delivery systems [1], DNA, mRNA [2,3] and peptide vaccines [4]. LNPs are crucial delivery systems that efficiently transport these components to specific cells. LNPs offer protection and stability to the encapsulated material during storage and transportation. They enhance cellular uptake by interacting with cell membranes and facilitate targeted delivery to the desired cells [5,6]. LNPs can be engineered to achieve controlled release, allowing for gradual and sustained delivery of genetic material or peptide antigens. This controlled release mechanism is beneficial in generating a robust and long-lasting immune response. LNPs possess biocompatible properties and can be customized to meet the specific requirements of different vaccines [7-9].

The size of LNPs significantly affects their efficiency in the desired applications [10]. The size criteria for LNPs are diverse. In drug delivery systems, the size of LNP ranges from 10 nm to 20 μm, depending on the drug delivery route [1]. LNPs utilized in vaccines require a size of 200 nm to attach to DC cells. Meanwhile, Hassett *et al.* [11], have exhibited that LNP sizes ranging from 60 - 150 nm can generate strong immune responses.

The self-assembly process of LNPs often lacks consistency in generating particles with uniform sizes, attributable to various factors such as AFR and N/P ratio. These inherent variabilities pose challenges in achieving the desired particle size range, underscoring the significance of parameter control for consistent outcomes and quality assurance [12]. Furthermore, the complexity is amplified by the selection of lipid composition and formulation parameters, as different lipids and excipients possess unique properties that can impact the final particle size [13].

The ideal sizes of the LNPs for vaccine development (60 - 150 nm) can be obtained by performing appropriate experimental optimization designs. The conventional experimental design uses the method of one factor at a time (OFAT) to obtain the optimum conditions for the involved factors [14]. In the OFAT method, each factor varies over its range, while other factors being constant at particular levels [15]. Despite being widely used in many research, OFAT does not consider possible interactions between factors, which may lead to failure in finding the true optimum condition [15,16]. Furthermore, OFAT is inefficient and requires many runs of experiments [16].

One of the modern strategies in experimental optimization is RSM, which varies all significant factors simultaneously [15]. RSM uses multivariate mathematics and statistics to find factor settings yielding an optimal response [15]. Unlike OFAT, RSM considers any interaction between factors. Therefore, RSM is suitable for finding the optimum factor settings [17]. In addition, it can minimize experimental costs and save time [18].

RSM has successfully assisted optimization in various fields [19]. Using RSM, Subramaniam *et al*. [19] optimized the formulation of nanostructured lipid carriers. Meanwhile, Hartati *et al.* [20], employed RSM to develop an aptasensor for hypertension.

RSM is a statistical approach that is commonly used to optimize process parameters and determine the optimal combination of variables [21]. In our study, RSM was employed to optimize the N/P ratio and AFR in order to enhance the efficiency of LNP production. RSM allows for the exploration of the response surface and the identification of the optimal operating conditions by fitting a mathematical model to experimental data [22,23]. The objective is to achieve particle size uniformity and essential factors for effective LNPs formulation. Through this optimization process, researchers can streamline the production of LNPs, minimizing variations and ensuring consistent, high-quality results. In the current study, we implemented RSM to find an optimal factor setting in the preparation of LNP containing pDNA. We used pDNA as a starting point before developing an mRNA vaccine due to its stability even at room temperature [24,25].

The size of LNPs is influenced by several factors, including the N/P ratio [26] flow rate ratio (FFR), and total flow rate (TFR) [10]. N/P is the ratio of the "N" amine group in ionizable lipids to the Phosphate "P" group in nucleic acids [27], whereas FRR is the ratio of aqueous-to-organic flow rate [28]. TFR is the summary of the aqueous and organic flow rates. We found that varying aqueous flow rates (AFRs) were more practical than FRRs (unpublished result). Therefore, in the present work, we optimize the size of LNPs-pDNA using RSM by varying the N/P Ratio and AFR. We fixed TFR 1 $mL.min^{-1}$, adopted from [29], because TFR is not a critical parameter according to [30].

Materials and methods

Materials

pDNA Human ACE-2 (Sino Biological), SM102 (Sinopeg), DSPC (Sinopeg), PEG-2000 (Sinopeg), Cholesterol (Nippon Fine Chemical Co., Ltd.), Sodium Citrate (Merck), Phosphate Buffer Saline (Sigma-Aldrich).

Instrumentation

Syringe Pump ICEN IN-G602 (ICEN Technology Company Limited), Staggered Herringbone mixer (SHM) (Microfluid chipshop), electrophoresis (Bio-rad), nanodrop2000 (Thermo Fisher Scientific), Zetasizer Nano Series (malvern panalytical).

Methods

Preparation of buffers

PBS was prepared by diluting the instant tablet in 200 mL of Aquadest sterile and adjusting the pH to 7.4 using NaOH or HCl [27,31]. Citrate buffer was made by mixing 5 mM sodium citrate, 5 mM citric acid, and 150 mM sodium chloride in aquadest sterile [27], and adjusting the pH to 3. TAE 1× buffer was prepared from TAE 50× buffer, which was made by weighing out 30.25 g of Tris-base and dissolving it in approximately 62.5 mL of Aquadest Sterile. Seven point one 5 mL of 100 % glacial acetic acid and 12.5 mL of 0.5 M EDTA (pH 8.0) were then added to the solution and the mixture was adjusted to a final volume of 125 mL using Aquadest sterile. The pH of this buffer should be around 8.5 without any adjustment and should be stored at room temperature. TAE 1× buffer was then obtained by diluting 20 mL of TAE 50× with Aquadest to a final volume of 1,000 mL. The final concentration of TAE 1× in the gel or running buffer will be 40 mM Tris, 20 mM acetic acid and 1 mM EDTA [32].

Isolation, characterization and quantification of plasmid pET28a-ACE2 from glycerol stock of *E. Coli* BL21(DE3)

The glycerol stock of *E. Coli* BL21(DE3) [pET28a-ACE2] was grown in 5 mL Luria Bertani medium containing kanamycin 25 ng.mL^{-1}, then incubated at 200 rpm, temperature 37 °C for 16 - 18 h. Harvesting and isolating the gene following the protocol from GenElute™ Plasmid Miniprep Kit (Sigma Aldrich).

The isolated plasmid of 5 µL was added with 1 µL of loading dye and 1 µL of gel red until the final volume was 7 µL. As a control, DNA markers were prepared by adding 4 µL NFW, 1 µL loading dye, 1 µL gelred and 1 µL DNA ladder 1 kb.

The isolated plasmids and markers were added to wells in a 1 % (w/v) agarose gel. The agarose gel was made by mixing 0.35 g of agarose with 35 mL of 1×TAE buffer. The mixture was then subjected to electrophoresis at a voltage of 80 V for 45 min, with 1×TAE buffer serving as the current-carrying medium.

The purity of the plasmid DNA isolate was determined by an absorbance ratio of 260/280 nm. The purity and concentration of plasmid DNA was determined using a NanoDrop 2,000 spectrophotometer (Thermo Scientific) [33].

N/P calculation

The N/P ratio is the total number of ionizable lipid amine groups (N) to the total number of negatively charged nucleic acid phosphate groups (P) [27]. According to Bailey-Hytholt *et al*. [27], the stages for calculating N/P include determining the number of N and P units, the nucleic acid mole and the mass concentration of nucleic acid. The number of N units was calculated using the Eq. (1) below:

$$N = Ionizable\ Lipid\ Concentration \times Lipid\ Mix\ Injection\ Volume \times Avogadro's\ Number\ x\ Number\ of\ N\ per\ Ionizable\ Molecule \quad (1)$$

The number of P units was determined as follows:

$$P = N \times x \quad (2)$$

where x is a desired value for the N/P ratio.

The nucleic acid mole was computed using the following formula (Eq. (3)):

$$The\ moles\ of\ Nucleic\ acid = \frac{P}{Avogadro's\ Number \times Number\ of\ P\ per\ Base\ pair \times Number\ of\ Bases} \quad (3)$$

where, the number of P units per base pair for DNA is 2.

The mass concentration of nucleic acid was calculated by employing the Eq. (4) below:

$$The\ mass\ concentration\ of\ Nucleic\ acid = \frac{Moles\ of\ Nucleic\ Acid \times Molecular\ Weight\ of\ Nucleic\ Acid}{Nucleic\ Acid\ Solution\ Injection\ Volume} \quad (4)$$

Because the stock of isolated pDNA produced is small, the lipid concentration must be adjusted to the desired N/P.

LNPs preparation and characterization

The mixture of lipid components was based on a molar ratio of 50:38.5:10:1.5 (SM102: Cholesterol: DSPC: PEG) [34] with a total stock lipid concentration of 10 mM in ethanol [27]. The final total lipid concentration was determined by the resulting N/P ratio. The lipid solution was sterilized using a 0.25 µm pore size filter. The pDNA isolate was solubilized using sterile citrate buffer. Encapsulation was performed by running the syringe pump at the desired flow rate. The LNPs mixture was placed in a tube containing 4×PBS. The LNPs were then measured using a Zetasizer according to standard operating procedures (SOP), including materials (LNPs and PBS), cell type (ZEN0118), temperature (25 °C), and 3 runs.

Optimizing LNPs using RSM

Constructions and data analyses of all experiment design matrices were performed in the R programming language [35], on the Jupiter-Notebook application [36]. The experimental factors used were the N/P ratio and the AFR, while the response was particle size. The 1st-order design consists of a 2-level full factorial and 4 center points, generated by the *FrF2* package [37]. The experiment results were analyzed to check the curvature using a 1st-order regression in the *rsm* package [38]. First-order regression model shows a lack of fit if the curvature is detected, indicating experimental conditions are close to the optimum region [15,16]. For optimizing the response, we used a central composite design (CCD) [39,40], generated using the *ccd* command in the *rsm* package. A 2nd-order regression was utilized to analyzed the CCD experiment results. The main effect plot was generated using the *FrF2* package, while contour and surface plots were created using the *plot* and *presp* commands, respectively, in the *graphics* package [35].

Results and discussion

Glycerol stock of *E. Coli* BL21(DE3) containing pDNA [pET28a-ACE2] was successfully grown, and [pET28a-ACE2] was isolated (**Figure 1**). ACE-2 gene was used as a dummy gene in this study.

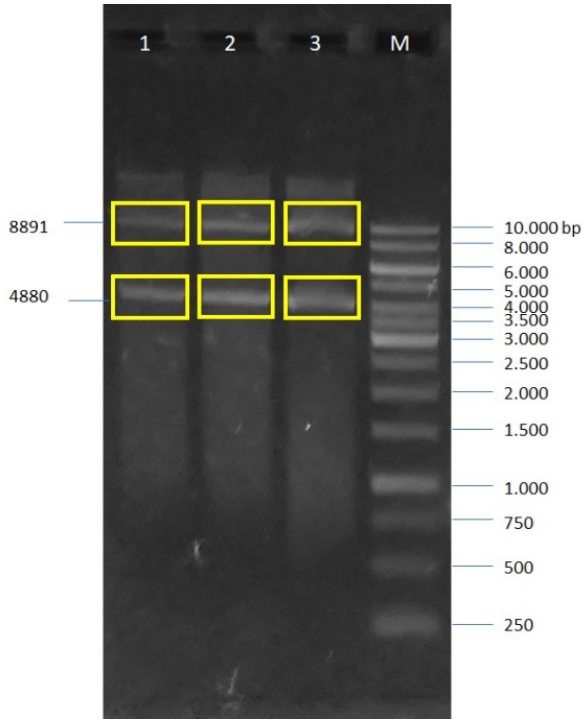

Figure 1 Agarose 1 % in TAE gel electrophoresis of [pET28a-ACE2]. Note: M: GeneRuler 1 kb DNA Ladder; 1: 1st tube of [pET28a-ACE2]; 2: 2nd tube of [pET28a-ACE2]; 3: 3rd tube of [pET28a-ACE2].

Based on agarose gel electrophoresis characterization (**Figure 1**), 2 bands emerged from the pDNA isolate. The bands that appear are supercoiled DNA (4,880 bp) and nicked DNA (8,891 bp) bands [41]. The isolation of pDNA resulted in more than a single band because it had not been linearized using restriction enzymes. The actual target pDNA size was 5,659 bp. The size of the target pDNA cannot be obtained accurately by the product instruction if there is no restriction on the pDNA.

Before using a DNA sample, the quality must be determined through the purity of the DNA. Absorbance ratios at 260 and 280 nm were used to assess DNA purity [42]. DNA purity is indicated by the absorbance ratio of 260/280 ~ 1.8 [43], 1.7 to 1.9 [44], or with an average value between 1.8 and 2.0 [45]. The pDNA used was purely based on the A260/A280 ratio value of 1.86 and had a concentration of 26.4 ng/µL. The pure isolate was dissolved into citrate buffer pH 3, which is commonly used to dissolve DNA in LNP manufacture [46].

The mixture of lipid components used was based on a molar ratio of 50:38, 5:10:1.5 (ionizable lipid: cholesterol: DSPC: PEG) [37,47]. Ionizable cationic lipids are vital in the self-assembly of LNPs containing nucleic acid. Additionally, they affect the structure and stability of LNPs and endosomal disruption. In this study, we utilized the ionizable lipid of SM-102 [48], which was previously successfully used in modern

vaccine formulations [49]. The SM-102 is conical in shape with a small head group and a broader cross-section of the molecule in the tail group incompatible with the lipid bilayer. Therefore, the endosome membrane's stability is disturbed, allowing the nucleic acid payload to be released to the cytosol [50]. Cholesterol is a helper lipid that enhances intracellular delivery and LNP stability *in vivo* [51]. Cholesterol had the highest LNP-mRNA encapsulation efficiency and the smallest size and polydispersity index (PDI) compared to other lipids [52]. DSPC is a phospholipid component that can balance the non-bilayer tendency of cationic lipids by providing a stable bilayer-forming structure. Previous research confirms that DSPC is localized mainly at the surface of mRNA-containing LNPs [53]. The central role of PEG is to form a steric barrier in the form of a hydrophilic layer on the surface of the nascent particles. PEG steric hindrance prevents inter-particle fusion and promotes the formation of a homogeneous population of LNPs, thereby contributing to storage stability [54].

Curvature check in the size optimization of LNPs containing pDNA

In this research, we optimized the size of lipid-encapsulated pDNA particles to achieve the LNP criterion (< 400 nm) [55] using 2 parameters: The N/P ratio and AFR. For the N/P ratio, we employed 8 and 32 as the low and high levels, respectively, according to the previous studies [16,17,40]. Meanwhile, the AFR levels of buffer and ethanol were set to 3:1, adapted from others [27,58] and 1:3 as a comparison. TFR was set constant at 1 $mL.min^{-1}$ [28]. A combination of the N/P ratio and AFR parameters generated a 2-level full factorial design. Additionally, 4 replicated center points were appended to the 2-level full factorial design to give adequate information about possible curvature in the surface response [61]. Adding 4 replicated center points to a 2-level full factorial design form a 1st-order design [15]. The center points used in our work were 20 and 0.5 $mL.min^{-1}$ for N/P AFR, respectively. The 1st-order design is useful to check a curvature in the RSM experiment [1538], based on the response represented by a linear function of the variables [60,61]. The run order of the design was randomized to reduce bias [62] and the influence of uncontrolled variables [63], during the encapsulation of pDNA by a lipid formulation using a staggered herringbone micromixer system [64].

Table 1 The size of lipid-encapsulated pDNA particles based on the experiment of 1st-order design.

NO	N/P	AFR*/ $mL.min^{-1}$	Polydispersity Index	Particle Size/ nm
1	20.0000	0.5000	0.216	270.30
2	20.0000	0.5000	0.190	262.70
3	32.0000	0.2500	0.272	865.70
4	8.0000	0.2500	0.112	633.80
5	20.0000	0.5000	0.177	338.80
6	32.0000	0.7500	0.188	147.10
7	8.0000	0.7500	0.365	381.10
8	20.0000	0.5000	0.286	328.90

Note: *AFR is the flow rate of DNA in aqueous solution with a total flow rate along with lipid in ethanol.

The resulting lipid-encapsulated pDNA particles were characterized using a dynamic light scattering (DLS) method [65]. Our results (**Table 1**) generally satisfied the LNP size requirement [55]. Nonetheless, for intravenous injection purposes requirement [55], only 1 preparation yielded an LNP with a particle size of 147.1 nm. It was obtained at an N/P of 32 and an AFR of 3:1. Increasing the N/P ratio decreases the size of LNPs [66] and raises transfection efficiency in gene delivery systems [67]. The best AFR obtained from the 1st-order experiment, aqueous/ethanol of 3:1, is consistent with other previous studies [27,50,68-69] where the lower lipid concentration tends to produce a small size of LNPs. In our experiment, we found the increased particle size when the AFR is 1:3, where lipid concentration is relatively high. This result has also been discussed by Maeki *et al*. [65].

Although the 1st-order experiment gave only 1 result that fulfills the LNP criterion, all the obtained data (**Table 1**) are very valuable for the curvature check for optimizing LNP size. The 1st-order regression model from those data reveals a significant lack of fit (p-value = 1.16×10^{-2}, α = 5 %) (**Table S1**), reflecting

that the parameter settings of LNP preparation are close to the optimum region. Furthermore, we also computed a model incorporating 1st-order and 2-way interaction terms. The acquired model was visualized into a contour (**Figure 2**(**A**)) and a 3-dimensional (3D) surface plot (**Figure 2**(**B**)).

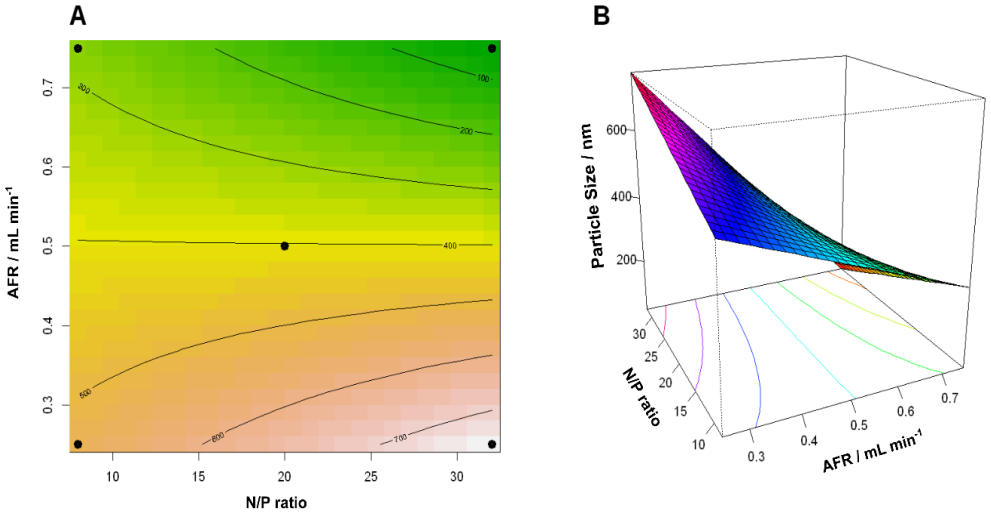

Figure 2 (A) Two-way interaction model visualized in contour and (B) 3D surface plots. The black dots in the corners and middle of the contour plot represent 2-level factorial design and center points, respectively.

In agreement with a significant lack of fit of the 1st-order model (**Table S1**), contour and 3D surface plots portray a curvature toward a minimum region (**Figures 2**(**A**) - **2**(**B**)), particularly around the N/P ratio of 30 and AFR of 0.75 mL.min^{-1}. Both graphs suggest that further experiments should explore the N/P ratio and AFR to produce smaller particle sizes beyond 30 and 0.75 mL.min^{-1}. In another study [27], the smallest LNPs were achieved by employing an N/P ratio of 36. Therefore, we constructed an experiment of central composite design (CCD) covering an N/P of 36 and AFR of more than 0.75 mL.min^{-1}.

Central composite design

To explore more regions around the parameter setting of AFR at 0.75 mL.min^{-1} and N/P ratio at 30, we constructed a CCD matrix using the *rsm* package. We set a new center point comprising an AFR of 0.75 mL.min^{-1} and an N/P ratio of 32. Six replicated center points were selected to give a uniform precision property of CCD [16]. For the low and high levels of the N/P ratio, we opted 27 and 37, respectively. This parameter setting covers an N/P ratio of 36. For the AFR, 0.6 and 0.9 mL.min^{-1} were chosen as the low and high levels to investigate the unexplored minimum region beyond 0.75 mL.min^{-1} (**Figures 2**(**A**) - **2**(**B**)). CCD also contains axial points, making the design rotatable [58]. The presence of center and axial points allows quadratic term estimation, which is vital for determining optimum conditions [16], in the LNP preparation. The CCD matrix for the experiment of lipid-encapsulated pDNA is shown in **Table 2**.

Table 2 The CCD matrix for lipid-encapsulated pDNA experiment and the resulting particle sizes.

NO	N/P	AFR/ mL.min^{-1}	Polydispersity Index	Particle Size/ nm
1	37.0000	0.6000	0.120	267.30
2	27.0000	0.9000	0.167	122.67
3	27.0000	0.6000	0.081	250.53
4	37.0000	0.9000	0.233	123.17
5	32.0000	0.7500	0.218	135.60
6	32.0000	0.7500	0.182	126.27
7	32.0000	0.7500	0.171	144.73

NO	N/P	AFR/ mL.min^{-1}	Polydispersity Index	Particle Size/ nm
8	32.0000	0.9621	0.314	104.00
9	32.0000	0.7500	0.177	127.23
10	39.0711	0.7500	0.230	140.77
11	32.0000	0.7500	0.376	162.80
12	32.0000	0.7500	0.128	125.90
13	32.0000	0.5379	0.143	324.13
14	24.9289	0.7500	0.171	139.30

According to the parameter conditions in the CCD matrix, as shown in **Table 2**, we performed a serial run of pDNA encapsulations, followed by particle size measurements. The acquired particle sizes are similar to the previous 1st-order experiment (**Table 2**). These results indicate that the parameter conditions are closer to the optimum. Furthermore, most of the lipid-encapsulated pDNA particles satisfy the size criterion of LNP, < 400 nm [55].

Subsequently, we fitted the 2nd-order model to the obtained data (**Table 2**). Although the 2nd-order model has relatively high residuals for runs 4 and 11 (**Table S2**), the lack of fit is insignificant (p-value = 4.82×10^{-1}, **Table S3**). Additionally, the quantile-quantile plot (**Figure S1**) depicts the normality of the residuals. These analyses show the adequacy of the 2nd-order model to the experimental data.

The 2nd-order model suggests that AFR significantly affects the particle size of lipid-encapsulated pDNA (p-value = 5.63×10^{-7}). In contrast, the N/P ratio values ranging from 24.9289 to 39.0711 do not influence the size of the resulting lipid-encapsulated pDNA (p-value = 6.48×10^{-1}). Both results are also in agreement with the main effect plots (**Figure 3**) which show no significant interaction between AFR and N/P ratio (p-value = 5.89×10^{-1}) (**Table S2**). It also suggests that only the AFR significantly affects the particle size of lipid-encapsulated pDNA (p-value = 5.63×10^{-7}).

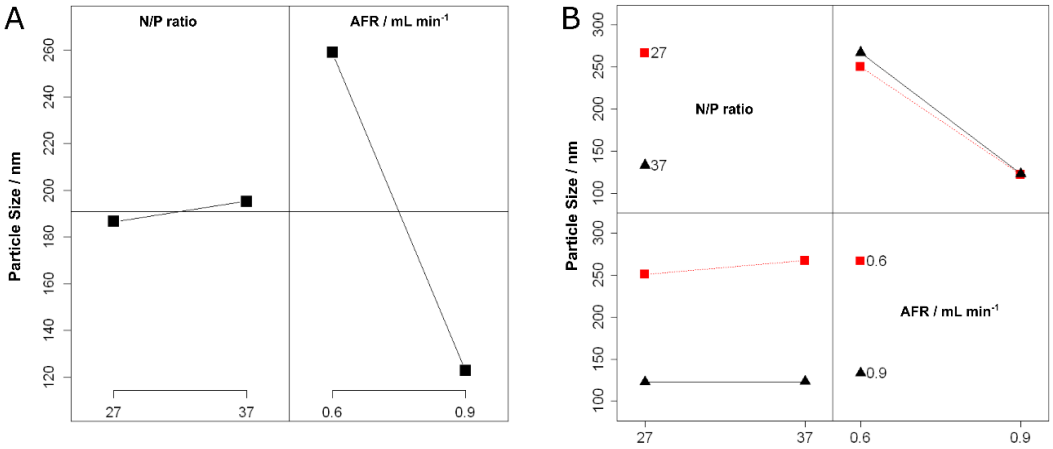

Figure 3 (A) Main effect and (B) interaction plots between the N/P ratio and AFR.

The regression coefficient for AFR is –72.9126 (Eq. (5)), meaning such a parameter has a main effect of 145.83 nm, 2nd-order model is as follows:

$$\hat{y} = 137.0883 + 2.4186x_1 - 72.9126x_2 + 4.0675x_1x_2 + 4.9402x_1^2 + 41.9552x_2^2 \quad (5)$$

where y denotes particle size, whereas x_1 and x_2 are the N/P ratio and AFR, respectively.

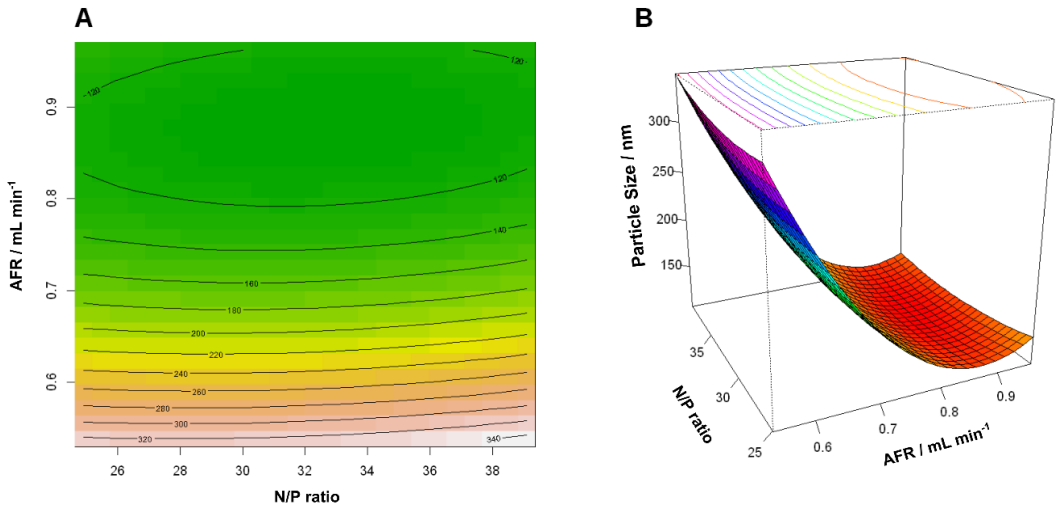

Figure 4 (A) Second-order model visualized in contour and (B) 3D surface plots.

The contour and 3D surface plots of the 2nd-order model clearly (**Figures 4**(**A**) - **4**(**B**)) reveal that parameter conditions have reached the optimum. The optimum conditions are characterized by circle or ellipse shape, where the valey stationary point is located. The 2nd-order model suggests a stationary point at N/P ratio of 32.58 and AFR of 0.88 mL/min. This stationary point is predicted to generate LNPs with sizes of 105.35 nm. Conducting an experiment using such a parameter condition is unessential in our case since smallest LNP has a particle size of 104.00 nm. This size of LNP was obtained by applying N/P ratio and AFR of 32 and 0.9621 mL/min. **Figure 4**(**B**) shows clearly that AFR significantly affects the particle size of LNP. In contrast, the N/P ratio within range of 24 and 39 do not influence the size of the resulting LNP. The N/P ratio may give a significant impact below 20 with the AFR values between 0.8 and 0.9, which can be expected from **Figures 4**(**A**) and **S2**.

According to the study, the size of LNPs is influenced by the AFR, which has been identified as a key factor. We provided evidence for this finding through experimental analysis. By systematically varying the flow rate ratio, we observed a consistent correlation between the flow rate ratio and LNP size. Specifically, increasing the AFR led to smaller LNP sizes. This significant impact of the flow rate ratio on LNP size was observed consistently across multiple experimental trials, establishing a strong influence of the AFR on LNP size.

Conclusions

We have implemented RSM to optimize the preparation parameters, including the N/P ratio and AFR, of LNP. We found that AFR significantly influence LNP size, whereas the N/P ratio did not significantly influence LNP size of 24.9289 to 39.0711. We also did not any interaction between both parameters in affecting LNP size. Assisting by RSM, we obtained an appropriate LNP size (104.00 nm) at the N/P ratio of 32.0000 and AFR of 0.9621 mL.min^{-1}. The findings of this study have significantly contributed to the acceleration of vaccine development by streamlining the preparation of LNPs. Moreover, the newfound ability to control LNP size offers immense potential for scalable manufacturing, ensuring consistent quality and enabling streamlined large-scale production. Overall, these remarkable findings provide a more effective and dependable method for LNP preparation, allowing researchers to focus their efforts on other crucial aspects of vaccine development and ultimately accelerating the production of effective vaccines.

Supporting information

Table S1 analysis of variance of the regression model of the 1st-order experiment (α = 5 %). **Table S2** The CCD matrix for lipid-encapsulated pDNA experiment and the resulting particle sizes complemented with their predicted and residual values. **Table S3** Analysis of variance of the quadratic model of CCD experiment (α = 5 %). FO denotes 1st-order, TWI 2-way interaction, and PQ pure quadratic. X1 and X2 are the N/P ratio and AFR, respectively. **Table S4**. Regression table of the quadratic model of CCD experiment (α = 5 %). **Figure S1**. Quantile-quantile plot of 2nd-order model residuals.

Acknowledgements

This research was supported by the RIIM LPDP Grant, grant number 44/IV/KS/06/2022. We also thanks to the Research Center of Molecular Biotechnology and Bioinformatics Universitas Padjadjaran and PT Bio Farma (Persero), Indonesia. The APC was funded by Universitas Padjadjaran, Indonesia.

References

[1] M Danaei, M Dehghankhold, S Ataei, FH Davarani, R Javanmard, A Dokhani, S Khorasani and MR Mozafari. Impact of particle size and polydispersity index on the clinical applications of lipidic nanocarrier systems. *Pharmaceutics* 2018; **10**, 57.

[2] FP Polack, SJ Thomas, N Kitchin, J Absalon, A Gurtman, S Lockhart, JL Perez, GP Marc, ED Moreira, C Zerbini, R Bailey, KA Swanson, S Roychoudhury, K Koury, P Li, WV Kalina, D Cooper, RWJ Frenck, LL Hammitt, Ö Türeci, H Nell, A Schaefer, S Ünal, DB Tresnan, S Mather, PR Dormitzer, U Şahin, KU Jansen and WC Gruber. Safety and efficacy of the BNT162b2 MRNA Covid-19 vaccine. *New Engl. J. Med.* 2020; **383**, 2603-15.

[3] LR Baden, HME Sahly, B Essink, K Kotloff, S Frey, R Novak, D Diemert, SA Spector, N Rouphael, CB Creech, J McGettigan, S Khetan, N Segall, J Solis, A Brosz, C Fierro, H Schwartz, K Neuzil, L Corey, P Gilbert, …, T Zaks. Efficacy and safety of the mRNA-1273 SARS-CoV-2 vaccine. *New Engl. J. Med.* 2021; **384**, 403-16.

[4] Y Fujita and H Taguchi. *Nanoparticle-based peptide vaccines*. Micro and nanotechnology in vaccine development. Elsevier Inc., Amsterdam, Netherlands, 2017, p. 149-70.

[5] X Han, H Zhang, K Butowska, KL Swingle, MG Alameh, D Weissman and MJ Mitchell. An ionizable lipid toolbox for RNA delivery. *Nat. Comm.* 2021; **12**, 7233.

[6] V Francia, RM Schiffelers, PR Cullis and D Witzigmann. The biomolecular corona of lipid nanoparticles for gene therapy. *Bioconjugate Chem.* 2020; **31**, 2046-59.

[7] MI Henderson, Y Eygeris, A Jozic, M Herrera and G Sahay. Leveraging biological buffers for efficient messenger RNA delivery via lipid nanoparticles. *Mol. Pharm.* 2022; **19**, 4275-85.

[8] S Feng, Z Wang, A Li, X Xie, J Liu, S Li, Y Li, B Wang, L Hu, L Yang and T Guo. Strategies for high-efficiency mutation using the CRISPR/Cas system. *Front. Cell Dev. Biol.* 2022; **9**, 803252.

[9] SA Dilliard and DJ Siegwart. Passive, active and endogenous organ-targeted lipid and polymer nanoparticles for delivery of genetic drugs. *Nat. Rev. Mater.* 2023; **8**, 282-300.

[10] M Maeki, Y Fujishima, Y Sato, T Yasui, N Kaji, A Ishida, H Tani, Y Baba, H Harashima and M Tokeshi. Understanding the formation mechanism of lipid nanoparticles in microfluidic devices with chaotic micromixers. *PLos One* 2017; **12**, e0187962.

[11] KJ Hassett, J Higgins, A Woods, B Levy, Y Xia, CJ Hsiao, E Acosta, MJ Moore and LA Brito. Impact of lipid nanoparticle size on MRNA vaccine immunogenicity. *J. Contr. Release* 2021; **335**, 237-46.

[12] A Moreno, J Liu, R Gueret, SE Hadi, L Bergström, A Slabon and MH Sipponen. Unravelling the hydration barrier of lignin oleate nanoparticles for acid- and base-catalyzed functionalization in dispersion state. *Angewandte Chemie* 2021; **60**, 20897-905.

[13] SM Moghimi, AC Hunter and JC Murray. Long-circulating and target-specific nanoparticles: Theory to practice. *Pharmacol. Rev.* 2001; **53**, 283-318.

[14] W Asad, T Kiran, F Saleem, S Siddiqui and SA Rasool. Co-optimization of *B. licheniformis* 208 biomass and alpha amylase synthesis using response surface methodology. *Pakistan J. Bot.* 2021; **53**, 2287-97.

[15] DC Montgomery. *Design and analysis of experiments*. 8th eds. John Wiley & Sons, New Jersey, 2013.

[16] J Lawson. *Design and analysis of experiments with R*. Chapman and Hall/CRC, New York, 2015.

[17] A Permana, HH Purba and S Hasibuan. Design of experiment (DOE) analysis with response surface method (RSM) to optimize the electroplating parameter. *ComTech* 2021; **12**, 99-109.

[18] A Doniavi, A Hosseini and G Ranjbary. Prediction and optimization of mechanical properties of St52 in gas metal arc weld using response surface methodology and ANOVA. *Int. J. Eng.* 2016; **29**, 1307-13.

[19] B Subramaniam, ZH Siddik and NH Nagoor. Optimization of nanostructured lipid carriers: Understanding the types, designs, and parameters in the process of formulations. *J. Nanoparticle Res.* 2020; **22**, 141.

[20] YW Hartati, DR Komala, D Hendrati, S Gaffar, A Hardianto, Y Sofiatin and HH Bahti. An aptasensor using ceria electrodeposited-screen-printed carbon electrode for detection of epithelial sodium channel protein as a hypertension biomarker. *Roy. Soc. Open Sci.* 2021; **8**, 202040.

[21] RH Myers, DC Montgomery and CM Anderson-Cook. *Response surface methodology: Process and product optimization using designed experiments*. John Wiley & Sons Inc., New Jersey, 2016.
[22] CE Mendoza-Chávez, A Carabin, A Dirany, P Drogui, G Buelna, MM Meza-Montenegro, RG Ulloa-Mercado, LM Díaz-Tenorio, LA Leyva-Soto and P Gortáres-Moroyoqui. Statistical optimization of arsenic removal from synthetic water by electrocoagulation system and its application with real arsenic-polluted groundwater. *Environ. Tech.* 2020; **42**, 3463-74.
[23] C Demirel, A Kabutey, D Herak, A Sedlaček, Č Mizera and O Dajbych. Using box-behnken design coupled with response surface methodology for optimizing rapeseed oil expression parameters under heating and freezing conditions. *Processes* 2022; **10**, 490.
[24] P Tebas, KA Kraynyak, A Patel, JN Maslow, MP Morrow, AJ Sylvester, D Knoblock, E Gillespie, D Amante, T Racine, T McMullan, M Jeong, CC Roberts, YK Park, J Boyer, KE Broderick, GP Kobinger, M Bagarazzi, DB Weiner, NY Sardesai and SM White. Intradermal SynCon® Ebola GP DNA vaccine is temperature stable and safely demonstrates cellular and humoral immunogenicity advantages in healthy volunteers. *J. Infect. Dis.* 2019; **220**, 400-10.
[25] S Stenler, P Blomberg and CIE Smith. Safety and efficacy of DNA vaccines: Plasmids vs. minicircles. *Hum. Vaccine. Immunotherapeutics* 2014; **10**, 1306-8.
[26] C Cayabyab, A Brown, G Tharmarajah and A Thomas. *mRNA lipid nanoparticles: Robust low-volume production for screening high-value nanoparticle materials*. Precision NanoSystems Inc., British Columbia, Canada, 2019.
[27] CM Bailey-Hytholt, P Ghosh, J Dugas, IE Zarraga and A Bandekar. Formulating and characterizing lipid nanoparticles for gene delivery using a microfluidic mixing platform. *J. Visual. Exp.* 2021; **168**, e62226.
[28] KH Moss, P Popova, SR Hadrup, K Astakhova and M Taskova. Lipid nanoparticles for delivery of therapeutic RNA oligonucleotides. *Mol. Pharm.* 2019; **16**, 2265-77.
[29] F Yanar, A Mosayyebi, C Nastruzzi, D Carugo and X Zhang. Continuous-flow production of liposomes with a Millireactor under varying fluidic conditions. *Pharmaceutics* 2020; **12**, 1001.
[30] T Terada, JA Kulkarni, A Huynh, S Chen, RVD Meel, YYC Tam and PR Cullis. Characterization of lipid nanoparticles containing ionizable cationic lipids using design-of-experiments approach. *Langmuir* 2021; **37**, 1120-8.
[31] Sigma-Aldrich. 10X Phosphate-Buffered Saline (PBS) for Western blotting, Available at: https://www.sigmaaldrich.com/ID/en/support/calculators-and-apps/10x-phosphate-buffered-saline, accessed March 2023.
[32] A Behle. Recipe for 50x TAE buffer, Available at: https://www.protocols.io/view/recipe-for-50x-tae-buffer-ewov1d47vr24/v1, accessed March 2023.
[33] AM García-Alegría, I Anduro-Corona, CJ Pérez-Martínez, MAG Corella-Madueño, ML Rascón-Durán and H Astiazaran-Garcia. Quantification of DNA through the nanodrop spectrophotometer: Methodological validation using standard reference material and Sprague Dawley rat and human DNA. *Int. J. Anal. Chem.* 2020, https://doi:10.1155/2020/8896738.
[34] M Qiu, Z Glass, J Chen, M Haas, X Jin, X Zhao, X Rui, Z Ye, Y Li, F Zhang and Q Xu. Lipid nanoparticle-mediated codelivery of Cas9 MRNA and single-guide RNA achieves liver-specific *in vivo* genome editing of Angptl3. *Proc. Natl. Acad. Sci. Unit. States Am.* 2021; **118**, e2018362118.
[35] R Core Team. *R: A language and environment for statistical computing*. R Core Team, Vienna, Austria, 2016.
[36] T Kluyver, B Ragan-Kelley, F Pérez, B Granger, M Bussonnier, J Frederic, K Kelley, J Hamrick, J Grout, S Corlay, P Ivanov, D Avila, S Abdalla and C Willing. Jupyter notebooks - a publishing format for reproducible computational workflows. *In*: Proceedings of the 20th International Conference on Electronic Publishing, Göttingen, Germany. 2016, p. 87-90
[37] UR Grömping. Package FrF2 for creating and analyzing fractional factorial 2-level designs. *J. Stat. Software* 2014; **56**, 1-56.
[38] R Lenth. V response-surface methods in R, using rsm. *J Stat Software* 2009; **32**, 1-17.
[39] S Bhattacharya. *Central composite design for response surface methodology and its application in pharmacy*. Response surface methodology in engineering science. IntechOpen, London, 2021.
[40] J Hao, F Wang, X Wang, D Zhang, Y Bi, Y Gao, X Zhao and Q Zhang. Development and optimization of baicalin-loaded solid lipid nanoparticles prepared by coacervation method using central composite design. *Eur. J. Pharmaceut. Sci.* 2012; **47**, 497-505.
[41] P Balagurumoorthy, SJ Adelstein and AI Kassis. Method to eliminate linear DNA from mixture containing nicked circular, supercoiled, and linear plasmid DNA. *Anal. Biochem.* 2008; **381**, 172-4.

[42] JA Glasel. Validity of nucleic acid purities monitored by 260nm/280nm absorbance ratios. *Biotechniques* 1995; **18**, 62-3.
[43] R Hassan, A Husin, S Sulong, S Yusoff, MF Johan, BH Yahaya, C Ang, S Ghazali and SK Cheong. Guidelines for nucleic acid detection and analysis in hematological disorders. *Malays. J. Pathol.* 2015; **37**, 165-73.
[44] Sigma-Aldrich. *GenElute™ plasmid miniprep kit*. Sigma-Aldrich, Missouri, 2013.
[45] G Lucena-Aguilar, AM Sánchez-López, C Barberán-Aceituno, JA Carrillo-Ávila, JA López-Guerrero and R Aguilar-Quesada. DNA source selection for downstream applications based on DNA quality indicators analysis. *Biopreservation Biobanking* 2016; **14**, 264-70.
[46] EM Mucker, PP Karmali, J Vega, SA Kwilas, H Wu, M Joselyn, J Ballantyne, D Sampey, R Mukthavaram, E Sullivan, P Chivukula and JW Hooper. Lipid nanoparticle formulation increases efficiency of DNA-vectored vaccines/immunoprophylaxis in animals including transchromosomic bovines. *Sci. Rep.* 2020; **10**, 8764.
[47] M Maugeri, M Nawaz, A Papadimitriou, A Angerfors, A Camponeschi, M Na, M Hölttä, P Skantze, S Johansson, M Sundqvist, J Lindquist, T Kjellman, IL Mårtensson, T Jin, P Sunnerhagen, S Östman, L Lindfors and H Valadi. Linkage between endosomal escape of LNP-mRNA and loading into EVs for transport to other cells. *Nat. Comm.* 2019; **10**, 4333.
[48] C Rae and NJ Thorwirth. *Systems and methods for decentralizing commerce and rights management for digital assets using a blockchain rights ledger*. Verimatrix Inc, California, 2017.
[49] H Steinle, A Behring, C Schlensak, HP Wendel, M Avci-Adali, SF Ahmed, AA Quadeer, MR McKay, NN Zhang, XF Li, YQ Deng, H Zhao, YJ Huang, G Yang, WJ Huang, P Gao, C Zhou, RR Zhang, Y Guo, SH Sun, …, M Jäättelä. International council for harmonisation (ICH) technical requirements for registration of pharmaceuticals for human use, E6(R2) Good Clinical Practice (GCP) guidance. *Viruses* 2020; **12**, 133-43.
[50] MJ Carrasco, S Alishetty, MG Alameh, H Said, L Wright, M Paige, O Soliman, D Weissman, TE Cleveland, A Grishaev and MD Buchmsnn. Ionization and structural properties of MRNA lipid nanoparticles influence expression in intramuscular and intravascular administration. *Comm. Biol.* 2021; **4**, 956.
[51] X Cheng and RJ Lee. The role of helper lipids in lipid nanoparticles (LNPs) designed for oligonucleotide delivery. *Adv. Drug Deliv. Rev.* 2016; **99**, 129-37.
[52] Y Eygeris, S Patel, A Jozic, G Sahay and G Sahay. Deconvoluting lipid nanoparticle structure for messenger RNA delivery. *Nano Lett.* 2020; **20**, 4543-9.
[53] MY Arteta, T Kjellman, S Bartesaghi, S Wallin, X Wu, AJ Kvist, A Dabkowska, N Székely, A Radulescu, J Bergenholtz and L Lindfors. Successful reprogramming of cellular protein production through MRNA delivered by functionalized lipid nanoparticles. *Proc. Natl. Acad. Sci. Unit. States Am.* 2018; **115**, E3351-E3360.
[54] BL Mui, YK Tam, M Jayaraman, SM Ansell, X Du, YYC Tam, PJ Lin, S Chen, JK Narayanannair, KG Rajeev, M Manoharan, A Akinc, MA Maier, P Cullis, TD Madden and MJ Hope. Influence of polyethylene glycol lipid desorption rates on pharmacokinetics and pharmacodynamics of siRNA lipid nanoparticles. *Mol. Ther. Nucleic Acids* 2013; **2**, e139.
[55] L Xu, X Wang, Y Liu, G Yang, RJ Falconer and CX Zhao. Lipid nanoparticles for drug delivery. *Adv. NanoBiomed Res.* 2021; **2**, 2100109.
[56] AK Blakney, PF McKay, BI Yus, Y Aldon and RJ Shattock. Inside out: Optimization of lipid nanoparticle formulations for exterior complexation and *in vivo* delivery of saRNA. *Gene Ther.* 2019; **26**, 363-72.
[57] J Wysocki, M Ye, E Rodriguez, FR González-Pacheco, C Barrios, K Evora, M Schuster, H Loibner, KB Brosnihan, CM Ferrario, JM Penninger and D Batlle. Targeting the degradation of angiotensin II with recombinant angiotensin-converting enzyme 2: Prevention of angiotensin II-dependent hypertension. *Hypertension* 2010; **55**, 90-8.
[58] MP Lokugamage, D Vanover, J Beyersdorf, MZC Hatit, L Rotolo, ES Echeverri, HE Peck, H Ni, JK Yoon, YT Kim, PJ Santangelo and JE Dahlman. Optimization of lipid nanoparticles for the delivery of nebulized therapeutic mRNA to the lungs. *Nat. Biomed. Eng.* 2021; **5**, 1059-68.
[59] MJ Anderson and PJ Whitcomb. *RSM Simplified: Optimizing processes using response surface methods for design of experiments*. 2nd ed. Productivity Press, New York, 2016.
[60] MW Mumtaz, A Adnan, H Mukhtar, U Rashid and M Danish. *Biodiesel production through chemical and biochemical transesterification: Trends, technicalities, and future perspectives*. Clean energy for sustainable development. Academic Press, London, 2017.

[61] AI Khuri. Response surface methodology and its applications in agricultural and food sciences. *Biometrics Biostatistics Int. J.* 2017; **5**, 155-63.
[62] AM García-Alegría, I Anduro-Corona, CJ Pérez-Martínez, MAG Corella-Madueño, ML Rascón-Durán and H Astiazaran-Garcia. Quantification of DNA through the nanodrop spectrophotometer: Methodological validation using standard reference material and Sprague Dawley rat and human DNA. *Int. J. Anal. Chem.* 2020; **2020**, 8896738.
[63] S Addelman. Statistics for experimenters. *Technometrics* 1979; **21**, 387-8.
[64] FL Vigario, NA Nagy, MH The, R Sparrius, JA Bouwstra, A Kros, W Jiskoot, ECD Jong and B Slütter. The use of a staggered herringbone micromixer for the preparation of rigid liposomal formulations allows efficient encapsulation of antigen and adjuvant. *J. Pharmaceut. Sci.* 2022; **111**, 1050-7.
[65] M Maeki, Y Fujishima, Y Sato, T Yasui, N Kaji, A Ishida, H Tani, Y Baba, H Harashima and M Tokeshi. Understanding the formation mechanism of lipid nanoparticles in microfluidic devices with chaotic micromixers. *Plos One* 2017; **12**, e0187962.
[66] K Kubota, K Onishi, K Sawaki, T Li, K Mitsuoka, T Sato and S Takeoka. Effect of the nanoformulation of siRrNAa-lipid assemblies on their cellular uptake and immune stimulation. *Int. J. Nanomedicine* 2017; **12**, 5121-33.
[67] Y Zhang, H Li, J Sun, J Gao, W Liu, B Li, Y Guo and J Chen. DC-Chol/DOPE cationic liposomes: A comparative study of the influence factors on plasmid pDNA and siRNA gene delivery. *Int. J. Pharm.* 2010; **390**, 198-207.
[68] N Kimura, M Maeki, Y Sato, Y Note, A Ishida, H Tani, H Harashima and M Tokeshi. Development of the ILiNP device: Fine tuning the lipid nanoparticle size within 10 nm for drug delivery. *ACS Omega* 2018; **3**, 5044-51.
[69] NM Belliveau, J Huft, PJ Lin, S Chen, AK Leung, TJ Leaver, AW Wild, JB Lee, RJ Taylor, YK Tam, CL Hansen and PR Cullis. Microfluidic synthesis of highly potent limit-size lipid nanoparticles for *in vivo* delivery of siRNA. *Mol. Ther. Nucleic Acids* 2012; **1**, e37.

Supplementary information for:
The implementation of response surface methodology in the optimization of lipid nanoparticle preparation for vaccine development

Table S1 Analysis of variance of the regression model of the first order experiment.

(α = 5%).

	Df	Sum Square	Mean Square	*F*-value	*p*
FO(x1, x2)	2	290122	145061	8.0494	2.73×10^{-2}
Residuals	5	90106	18021		
Lack of fit	2	85492	42746	27.7939	1.16×10^{-2}
Pure error	3	4614	1538		

Table S2 The CCD matrix for lipid-encapsulated *p*DNA experiment and the resulting particle sizes complemented with their predicted and residual values.

No	N/P ratio	Aqueous Flow Rate (mL/min)	Ethanol Flow Rate (mL/min)	Particle Size (nm)	Predicted Particle Size (nm)	Residual (nm)
1	37.0000	0.6	0.4	267.3	263.3825	3.917534
2	27.0000	0.9	0.1	122.67	112.72	9.949966
3	27.0000	0.6	0.4	250.53	250.4102	0.119758
4	37.0000	0.9	0.1	123.17	109.4223	13.74774
5	32.0000	0.75	0.25	135.6	137.0883	-1.48833
6	32.0000	0.75	0.25	126.27	137.0883	-10.8183
7	32.0000	0.75	0.25	144.73	137.0883	7.641667
8	32.0000	0.9621	0.0379	104	117.8848	-13.8848
9	32.0000	0.75	0.25	127.23	137.0883	-9.85833
10	39.0711	0.75	0.25	140.77	150.3892	-9.61918
11	32.0000	0.75	0.25	162.8	137.0883	25.71167
12	32.0000	0.75	0.25	125.9	137.0883	-11.1883
13	32.0000	0.5379	0.4621	324.13	324.1127	0.017257
14	24.9289	0.75	0.25	139.3	143.5483	-4.24832

Table S3 Analysis of variance of the quadratic model of CCD experiment (α = 5%). FO denotes first-order, TWI two-way interaction, and PQ pure quadratic.

X1 and X2 are the N/P ratio and AFR, respectively.

	Df	Sum Square	Mean Square	*F*-value	*p*
FO(x1, x2)	2	42577	21288.4	102.1130	2.02×10^{-6}
TWI(x1, x2)	1	66	66.2	0.3174	5.88×10^{-1}
PQ(x1, x2)	2	13020	6510.2	31.2274	1.66×10^{-4}
Residuals	8	1668	208.5		
Lack of fit	3	607	202.2	0.9530	4.82×10^{-1}
Pure error	5	1061	212.2		

Table S4 Regression table of the quadratic model of CCD experiment (α = 5%).

	Estimate	**Std. Error**	***t*-value**	***p***
(Intercept)	137.0883	5.8946	23.2566	1.24×10^{-8}
x1	2.4186	5.1049	0.4738	6.48×10^{-1}
x2	-72.9126	5.1049	-14.2829	5.63×10^{-7}
x1:x2	-4.0675	7.2194	-0.5634	5.89×10^{-1}
$x1^2$	4.9402	5.3133	0.9298	3.80×10^{-1}
$x2^2$	41.9552	5.3133	7.8962	4.80×10^{-5}

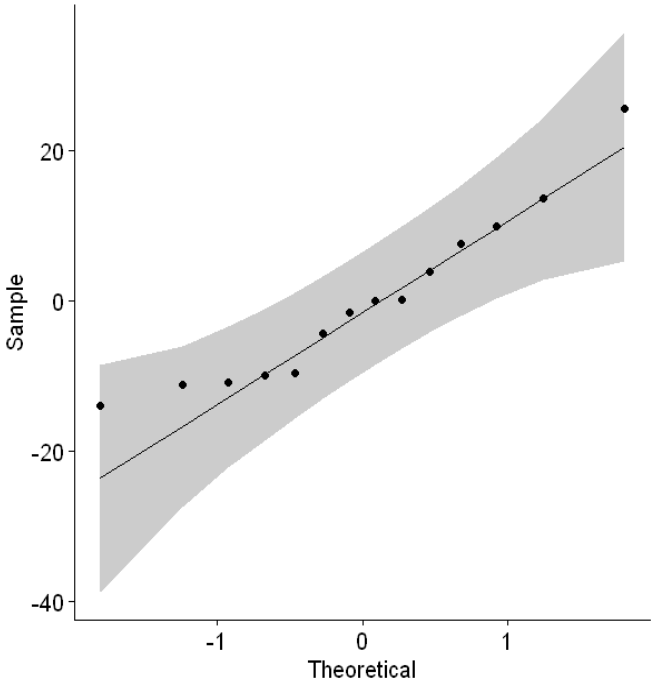

Figure S1 Quantile-quantile plot of second-order model residuals.

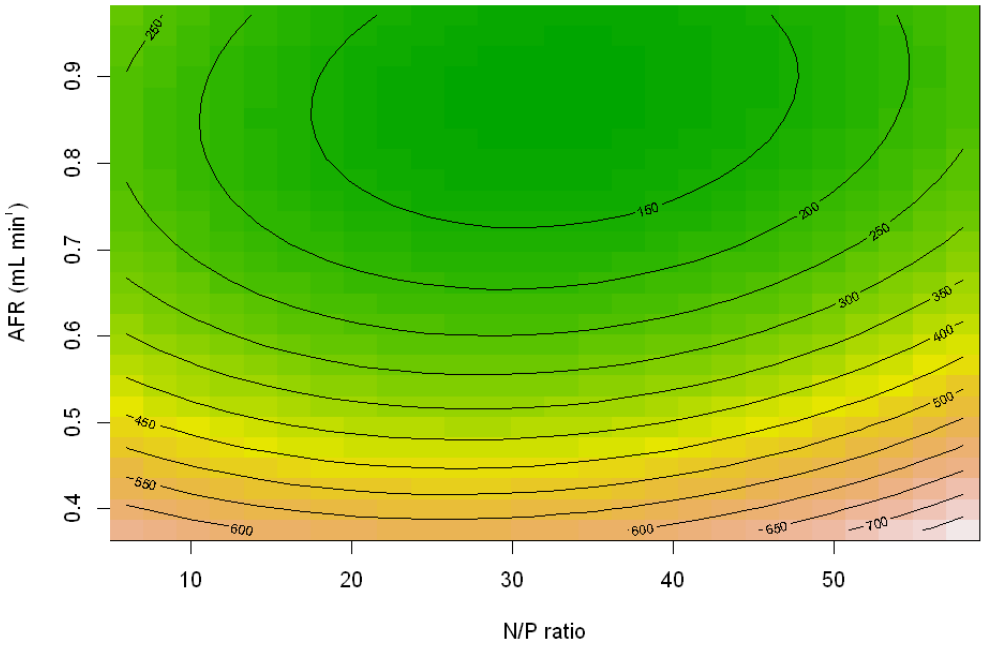

Figure S2 Expanded contour plot for the second-order model.